LASER & PHOTONICS REVIEWS

www.lpr-journal.org

Inverse-Designed Integrated Nonlinear Optical Switches

Hao Chen, Jiatong Li, Zhenyuan Shang, Guoqing Wang, Ziming Zhang, Zexing Zhao, Mengyu Zhang, Jinde Yin, Jinzhang Wang, Kai Guo, Junbo Yang, and Peiguang Yan**

Due to the slowdown of Moore's law, the integrated photonic devices have provided a route to promote the development of large-scale optical communications with high performance. As one of the essential components of optical routers, an optical switch can fast transmit or block the optical signal. However, most of the integrated optical switches reported to date rely on thermo-, magneto-, or electro-optical effects, which limit applications due to slow response times, large footprint, and complexity fabrication. Here, an integrated nonlinear optical switch designed by the inverse-design method and fabricated on the SiN platform is introduced. The integrated optical switch is demonstrated with significant intensity-dependent transmission at 1.5 μm waveband. The polarization-depended capability is explored by using fundamental polarized lights (transverse electric and transverse magnetic, respectively), which exhibits opposite transmission change trends during the whole power range and opens potential applications such as photonic quantum information processing. In order to address the saturation of Kerr-nonlinearity in SiN materials at high power, a MoS_2/SiN hybrid integrated optical switch is fabricated by uniformly cladding few-layer MoS_2 on the surface of inverse-designed region. That is demonstrated to enhance the nonlinear optical response of device efficiently and achieve more excellent switching capability at high power.

1. Introduction

Large-scale optical communication and data center are playing a more and more important role in various fields including big data analytics and cloud computing.[1–4] With the advances in complementary metal oxide semiconductor (CMOS) compatible silicon photonics in recent years, low-cost and small footprint, such as micro-ring resonators (MRRs) and Mach–Zehnder interferometers (MZIs) have enabled integrated optical networks for a wide range of applications, including multiprocessor systems-on-chip, and rack-to-rack connections.[5–7] The number of processors in a server rack can be very large and growing, requiring high-radix optical networks to support the exchange of information among hundreds or thousands of communication nodes. Generally, an optical signal needs to pass numerous optical routers and crossings from input to output, which always introduces a large amount of accumulated loss.[8]

To date, integrated optical routers have been developed on various CMOS compatible platforms such as silicon on insulator (SOI), silicon nitride (SiN), and lithium niobate (LN) through the application of electro-optical, thermo-optical, or electro-mechanical effects.[9–12] As one of the key components of an optical router, optical switch can transmit or block the optical signal depending on the routing protocol.[13] The controlled alteration of the phase and absorption of propagation light has been utilized to the design of integrated optical switches. However, the major challenge in the traditional optical switches is the absence of low-loss, small footprint, and ultrafast switching technology, which is required for large-capacity optical communications to route the optical signal among different optical channels. For instance, optical switches relied on thermo-optic effect suffer from high power-consumption, slow response time (typically <10 kHz), and large interaction length between optical waveguide and micro-heater. Integrated optical switches depended on electro-optical effect (e.g., plasma dispersion effect) are limited by low modulation-efficiency and large carrier-induced loss.[14,15] Moreover, since the exploration of traditional optical switches (such as MRRs and MZIs) is mainly based on human-intuition, the limiting character of human-based intuition for the design of improved nanoscale devices is apparent when considering the tremendous control over topology and composition of nanophotonic structures allowed by state-of-the-art nanofabrication techniques.[16,17] The optimization of traditional optical devices largely relies on experience of the design templates, and owing to constraints on simulation power and time, only limited design parameters are

H. Chen, J. Li, Z. Shang, G. Wang, Z. Zhang, Z. Zhao, M. Zhang, J. Yin, J. Wang, P. Yan
College of Physics and Optoelectronic Engineering
Shenzhen University
Shenzhen 518060, China
E-mail: yanpg@szu.edu.cn

K. Guo
Institute of Systems Engineering
Academy of Military Science
Beijing 100039, China
E-mail: guokai07203@hotmail.com

J. Yang
College of Liberal Arts and Sciences
National University of Defense Technology
Changsha 410000, China

The ORCID identification number(s) for the author(s) of this article can be found under https://doi.org/10.1002/lpor.202200254

DOI: 10.1002/lpor.202200254

adjusted in searching for the optimal structure. Therefore, it is essential to find an alternative approach to further explore the performance of integrated optical switches.

Recently, an introduced alternative relies on inverse-design integrated optical switches combined with the Kerr-nonlinearity. Different from the above-mentioned effects, the Kerr effect is instantaneous, which can contribute to design optical switch with ultrafast response capability. Furthermore, inverse design, meaning the direct retrieval of the proper structure for the desired optical performance, enables to explore a much larger degrees of freedom in the design space and has attracted increasing attention as a powerful approach to go beyond human-intuition based optical devices.[18–20] Recently, Hughes et al. has proposed an efficient gradient-optimization algorithm combined with adjoint method to investigate the Kerr-nonlinearity in integrated photonics.[21] The simulated results demonstrate that the inverse-designed optical switch shows remarkable nonlinear optical performances, which uses chalcogenide glass (Al_2S_3) as the Kerr medium and is operated at 2 μm waveband. However, so far, there are few experimental reports on the performance of inverse-designed nonlinear optical switches, which is greatly important for the practical applications of this type of nonlinear devices. Moreover, 2D layered materials (2DLMs), such as graphene and transition metal dichalcogenides (TMDCs), have been demonstrated with remarkable nonlinear optical properties such as nonlinear frequency conversions, ultrafast saturable absorption, and optical modulation.[22–25] Specifically, as one of the typical members in TMDCs family, molybdenum disulfide (MoS_2) has a crystal lattice structure comprised a layer of hexagonally arranged molybdenum atoms covalently sandwiched between two layers of sulfur atoms. Since the MoS_2 layer is terminated with sulfur atoms without dangling bonds and adjacent layers are weakly bound together by van der Waals forces, which leads to remarkable chemical stability and enables to engineer various heterostructure devices by vertical transferring technology.[26–28] The previous researches reported that MoS_2 has an effective optical Kerr coefficient of about 1.1×10^{-16} m^2 W^{-1}, which is near three orders of magnitude higher than that of the SiN (2.5×10^{-19} m^2 W^{-1}).[29] Therefore, it is appealing to the hybrid integration of the excellent nonlinear optical properties of MoS_2 film with high-quality optical waveguides to further explore the nonlinear optical performance of the integrated optical switches.

In this work, we propose an integrated nonlinear optical switch designed by using gradient-optimization algorithm combined with adjoint method and fabricated on the SiN platform. The proposed optical switch has an extremely compact footprint (5.75 × 5.75 $μm^2$) and is experimentally demonstrated with excellent intensity-dependent transmission property. Specifically, the transmission of output port can be efficiently modulated at different incident powers, which can be mainly divided into two states with 13.56% and 9.09% modulation depth, respectively. Interestingly, the inverse-designed optical switch also shows significant polarization-dependent property, which has opposite transmission change trends at different polarized lights (transverse electric (TE) and transverse magnetic (TM) polarization, respectively) and displays the saturation of the Kerr-nonlinearity at TM polarized incident light. In order to overcome the limitation of the nonlinear saturation of the Kerr effect, a MoS_2/SiN hybrid integrated optical switch is prepared by hybrid integrating few-layer MoS_2 on the surface of inverse-designed region. Compared with the optical switch realized by the Kerr-nonlinearity of the SiN material itself, the MoS_2/SiN hybrid integrated optical switch shows stronger nonlinear modulation capability and no saturation is observed even at the maximum incident power. This is the first experimental demonstration of integrated nonlinear optical switches based on inverse design and Kerr-nonlinearity to the best of our knowledge. The results indicate that the proposed approach opens an exciting platform to explore novel nonlinear integrated devices, which have potential applications in nonlinear optics, optical communications, and large-scale integrated photonic circuits.

2. Inverse Design and Simulation

The structure distribution of integrated optical switch is automatically computational optimization by using gradient-optimization algorithm combined with adjoint method (open-source package named "angler").[21] Specifically, the simulated width of bus waveguide is set to be 1.2 μm, which enables to support fundamental modes with a low propagation loss. The inverse-designed region has a 5.75 μm × 5.75 μm (length × width) size. The initial propagation light is set to be fundamental TM polarization. **Figure 1**a is the finally optimized permittivity distribution at the inverse-designed region, which has one input port (red arrow) and two output ports. The input port is used to couple the incident light into the inverse-designed region. The target of the optimization process is to find a maximum value of the objective function to maximize the transmission in the bottom output port (blue arrow) at the low incident power (linear regime) while achieving largest transmission in the right output port (green arrow) at the high incident power (nonlinear regime) relied on the Kerr-nonlinearity. Figure 1b is the relationship between the objective function and iteration numbers. The total iteration number is set to be 500, considering the performance of device and the computing time. The maximum objective function is reached to 0.912 while the maximum value of objective function is normalized to 1 in the simulated result. The inset image is the optical field distribution at the linear (blue) and nonlinear (orange) regime, respectively. Specifically, when the intensity of the incident light exceeds the threshold of nonlinear optical response, the transmission of the port 2 is increased obviously caused by the Kerr effect.

3. Sample Fabrication and Experimental Setup

Figure 2a is the schematic of our integrated optical switch. Note that the thick SiN (≈780 nm thickness) is utilized as the Kerr nonlinear medium in our experiment. Thick SiN has been demonstrated with enormous physical properties, such as high refractive index to confine the incident light into a tiny waveguide with ultralow propagation loss, large nonlinear coefficient to generate different nonlinear phenomenon and CMOS compatible with low-cost. Different integrated photonic devices have also been developed on the thick SiN platform such as Kerr optical frequency combs, high-speed modulators, and microwave processing photonic circuits.[30–32] The inverse taper is used as a mode transformer to ensure a high coupling efficiency between the external

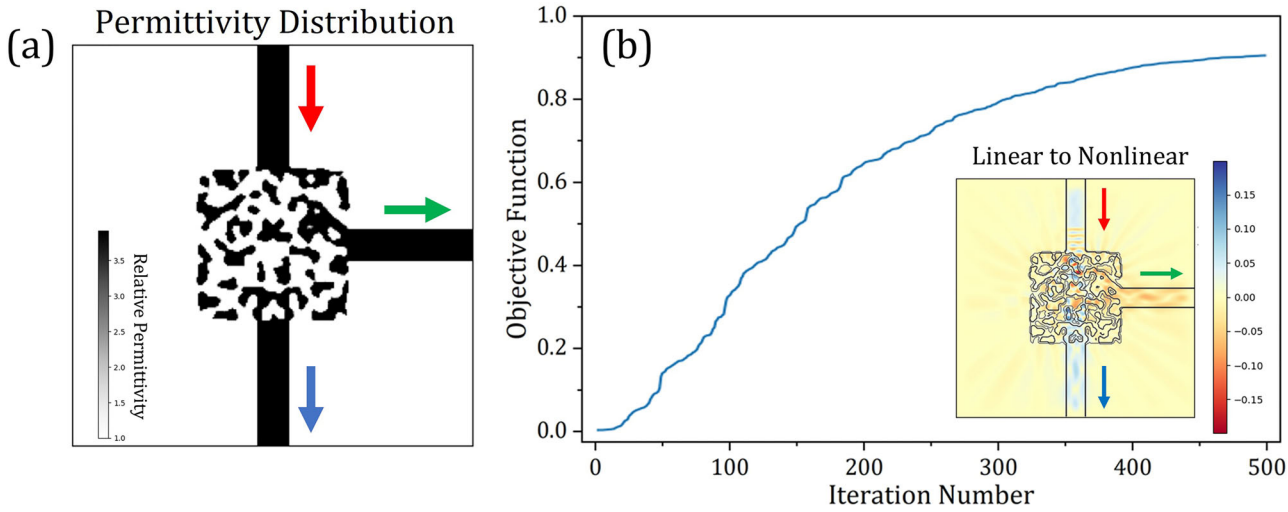

Figure 1. a) The inverse-designed permittivity distribution of the integrated optical switch, which has one input port (red arrow) and two output ports. The inverse-designed region is optimized to maximize the transmission of the right output port (green arrow) at high incident power while the bottom output port (blue arrow) at low incident power. b) The objective function under different iteration numbers. Note that the initial propagation light is set to be fundamental TM polarization. Inset image is the optical field distribution with the linear to nonlinear optical response, respectively.

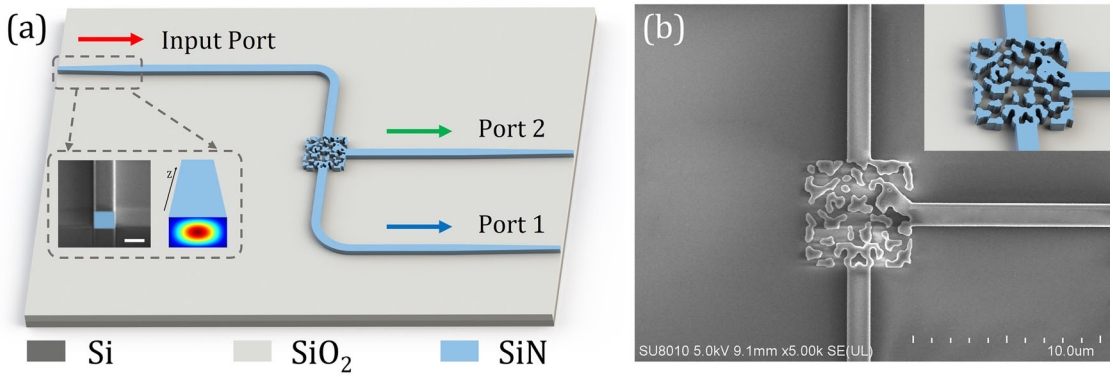

Figure 2. a) The schematic of the integrated optical switch. The inverse tapers are used as mode transformers to enhance the coupling efficiency between external lensed fiber and SiN waveguide at both sides. The inset images are the SEM of the cross section of the SiN waveguide, which has a ≈88.9° sidewall verticality and smooth surface that can contribute to the low propagation loss. The optical field distribution of the fundamental mode is simulated by using FDTD method. Scale bar: 1 μm. b) The SEM of the inverse-designed region. The inset image is the schematic of inverse-designed region after the optimization.

lensed fiber and the SiN bus waveguide at the input and output. The cross section of the inverse taper is optimized to be 350 nm × 780 nm (width × height), and the taper length is optimized to be 350 μm.[33] The SiN bus waveguide has a 1.2 μm × 780 nm (width × height) cross section. As shown in the inset image of Figure 2a, the fundamental mode is well confined inside the SiN waveguide. The scanning electron microscope (SEM) image of the cross section of the SiN waveguide indicates that the optical waveguide has an ≈88.9° sidewall verticality and smooth surface that are benefited for the low propagation loss of the fundamental modes. Furthermore, the optical field distributions at different incident powers are simulated by using finite-difference time-domain (FDTD) method (Figure S1, Supporting Information), which shows obviously different propagation paths at linear regime and nonlinear regime, respectively. Note that slight optical field scattering can be reduced by further optimizing the algorithm parameters and increasing the number of iterations. Figure 2b is the SEM image of inverse-designed region, which is well consistent with the optimized results to ensure remarkable nonlinear optical performance. Thanks to the final inverse-designed region only has a 5.75 × 5.75 μm^2 size, which is much smaller than conventional integrated optical devices (e.g., MRRs and MZIs) and contributes to reduce the system volume and the fabrication complexity of the large-scale integrated photonic circuits. The experimental setup is shown in **Figure 3**. A mode-locked ultrafast fiber laser is used as the 1.5 μm light source with ≈200 fs pulse duration and 80.47 MHz repetition rates. The round-trip time of pulse train is measured to be 12.4 ns (Figure S2a, Supporting Information). The signal to noise ratio of output pulse train is measured to be 82.8 dB, indicating a stable and low-noise state of pulsed laser (Figure S2b, Supporting Information). In order to ensure the performance of the pulsed laser

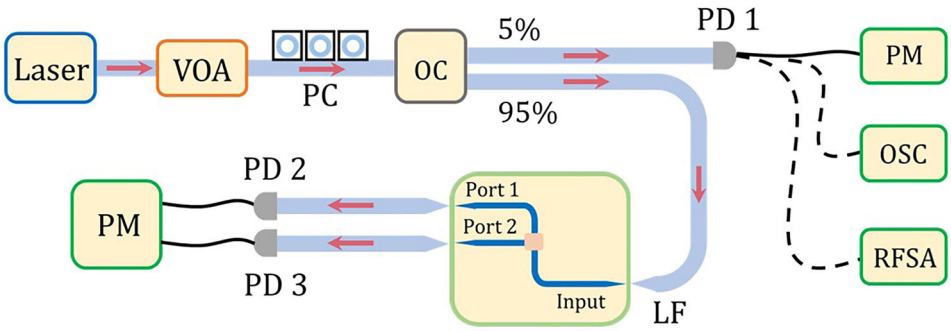

Figure 3. Schematic diagram of the experimental setup. VOA: variable optical attenuator; PC: polarization controller; OC: optical coupler; PD: photodetector; PM: power meter; OSC: oscilloscope; RFSA: radio frequency spectrum analyzer; LF: lensed fiber.

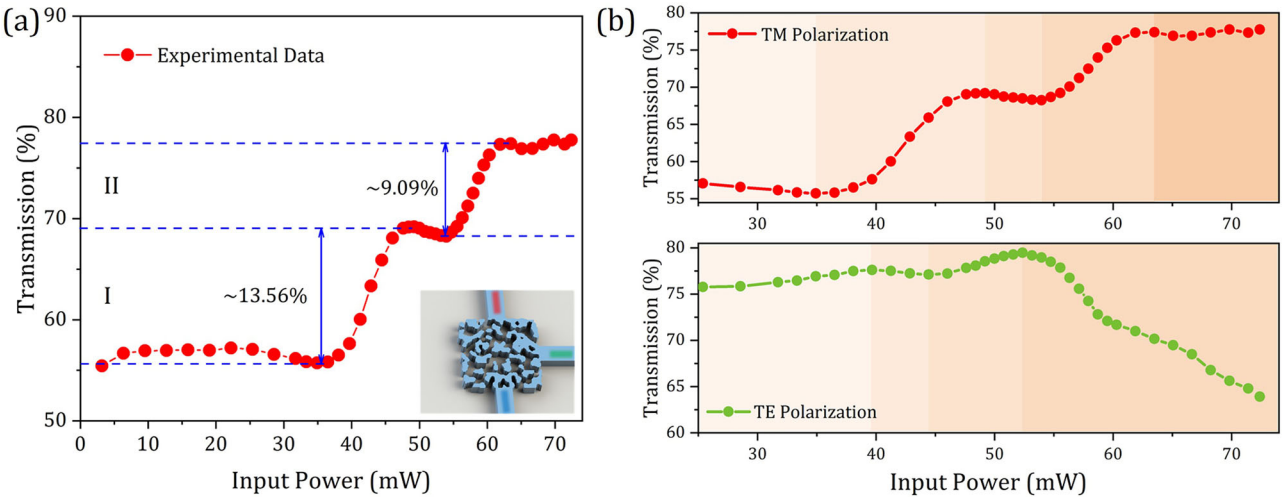

Figure 4. a) The transmission of TM polarized light to port 2 at different incident powers. Inset image is the schematic of inverse-designed structure with one input port (red) and two output ports (blue and green). b) Comparison of transmission curves of port 2 at TM and TE polarized incident lights, respectively. The gradient background colors represent different nonlinear optical response states.

during the experimental measurement, a variable optical attenuator is used to modulate the coupling power between the external laser and SiN waveguide to characterize the intensity-dependent performance of the integrated optical switch. A polarization controller (PC) is utilized to adjust the polarization of the incident light.

4. SiN Based Integrated Optical Switch

Figure 4a shows the transmission curve of port 2 at different incident powers. The transmission of the port 2 is measured to be ≈55.6% when the incident power is lower than 34.91 mW. However, when the incident power exceeds 34.91 mW (corresponding to the threshold of nonlinear optical response), the port 2 occurs a significant intensity-dependent transmission curve. Specifically, the total transmission curve of port 2 can be mainly divided into two switching states. At the first state I, when the incident power is adjusted ranging from 34.91 to 48.6 mW, the modulation depth of inverse-designed optical switch is calculated to be ≈13.56%. Then the transmission of port 2 shows a stage with a slight transmission drop from 69.1% (48.6 mW) to 68.3% (53.96 mW). When the incident power is further increased, the transmission of port 2 is subsequently increased to 77.5% with a ≈9.09% modulation depth (second state II) and then exhibits a saturation phenomenon. The results indicate that inverse-designed optical switch possesses a remarkable intensity-dependent switching capability. Furthermore, the previous researches have demonstrated that the Kerr-nonlinearity is typically phase sensitive, therefore a proper phase relationship (phase matching) are required to obtain efficient nonlinear optical response.[22] Since the optical switch used in our experiment is optimized at the TM polarized light, the nonlinear optical response at different polarizations is experimentally measured to further explore the polarization-dependent properties of the inverse-designed optical switch. As shown in Figure 4b, when the incident light is set to be the TE polarization and the incident power is below the threshold of nonlinear optical response, the port 2 has a larger transmission value (75.8%) than that of incident light with a TM polarization (57.3%), which is mainly caused by the different polarization propagation losses in the SiN bus waveguide and inverse-designed region. The significant nonlinear optical response of the optical switch can be only observed at the incident light with the pure TM polarization, which is also consistent with the target of the maximum objective function optimization (increasing

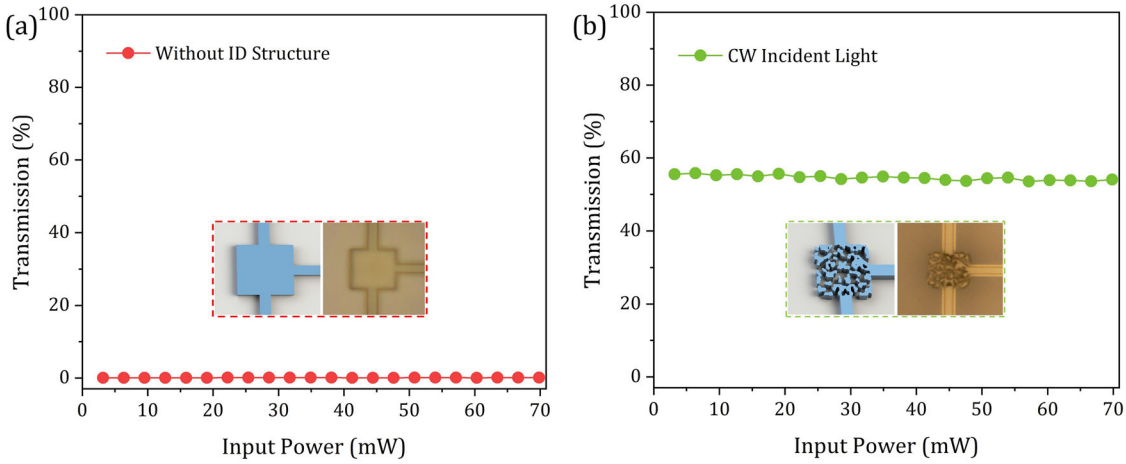

Figure 5. a) The transmission of port 2 without inverse-designed region. b) The transmission of port 2 with a CW incident light. The inset images are the schematic of inverse-designed region with and without inverse-designed structure and the optical images of fabricated devices, respectively.

the transmission of port 2 under high output powers). Interestingly, when the polarization of incident light is set to be the TE polarization, the inverse-designed optical switch shows opposite transmission change trends compared to the transmission at the TM polarization. In detail, although the ranges of incident power for each nonlinear optical response states are slightly different, the change trends of transmission maintain the opposite before the last nonlinear optical response state, which shows a near constant transmission (≈77.5%) at the TM polarization while it's dropped from 72.1% to 65.6% at the TE polarization. The results indicate that inverse-designed optical switch owns significant polarization-dependent properties, which might be used in various applications such as on-chip laser, and photonic quantum information processing.

In order to demonstrate the nonlinear transmission properties of optical switch is caused by the inverse-designed region combined with Kerr-nonlinearity, we fabricate a same size square without inverse-designed structure. As shown in **Figure 5**a, the inset images are the schematic and the optical image of the fabricated device. During the incident power of pulsed laser adjusted ranging from 0 to 70 mW, the transmission of port 2 remains at zero, indicating that there is no light guided into the port 2. Furthermore, a continue-wave (CW) laser with 200 kHz linewidth at the central wavelength of 1550.12 nm is used to examine the nonlinear optical performance of the inverse-designed optical switch. The maximum output power of CW laser is amplified to 100 mW by an erbium-doped fiber amplifier. Figure 5b shows that the transmission of port 2 is always at ≈55.6%. No significant nonlinear changes of transmission curve are observed over the entire power range. The experimental results demonstrate that the switching capability of integrated nonlinear optical switch is caused by the inverse-designed region in cooperated with the Kerr-nonlinearity. Furthermore, note that the previous research reported that the response time of Kerr effect in SiN belongs to a few femto-second time scale, indicating that our inverse-designed optical switch owns the potential to achieve sub-nanosecond response.[34] That is critical to meet the ultracompact footprints and low-latency requirements posed by future large-scale optical communication and cloud workloads.[35]

5. MoS_2/SiN Hybrid Integrated Optical Switch

The few-layered MoS_2 film with large-area is first grown via chemical vapor deposition method. By using chemically assisted wet transfer method, MoS_2 film with large-area is then uniformly transferred on the surface of inverse-designed region to form a van der Waals heterostructure (vdWh). The optical images of inverse-designed optical switch before and after few-layer MoS_2 cladding are shown in Figure S3a,b, Supporting Information, indicating MoS_2 film uniformly cladded on the surface of inverse-designed region. No significant wrinkling or tearing is observed in the cladding area, ensuring an efficient interaction between the propagation light and the MoS_2 film without large scattering losses. The Raman spectrum of few-layer MoS_2 after transfer is recorded using 532 nm laser line and shows two typical Raman vibrable modes (E^1_{2g} and A_{1g}, respectively), which indicates a high-crystal-quality of MoS_2 film cladded on the surface of inverse-designed region and minimizes the impact of external factors (e.g., defects, strains, and chemical treatment) on the material nonlinear optical performance (Figure S4, Supporting Information). The linear transmittance curve of few-layer MoS_2 is measured by using a UV–vis/near-infrared spectrometer with 1 nm steps. The linear absorption of few-layer MoS_2 used in our experiment is measured to be 5.32% at 1550 nm (Figure S5, Supporting Information). Low linear absorption of few-layer MoS_2 can help reduce the insertion loss introduced by the MoS_2 film when engineering hybrid structures (MoS_2/SiN).

As shown in **Figure 6**a, the inset image is the schematic of inverse-designed optical switch cladded with few-layer MoS_2 film. The transmission curve of port 2 is observed with similar transmission trends compared to the optical switch without MoS_2 film cladding. Specifically, at the first state I, the threshold of nonlinear optical response is measured to be 34.91 mW, which is same as the optical switch without MoS_2 cladding. Then the transmission of port 2 shows a clear stage with a transmission drop from 58.27% (44.3 mW) to 57.4% (49.2 mW). Note that the value of transmission change and the range of incident power are very close between optical switch with and without MoS_2 cladding, indicating that this drop is mainly caused by the

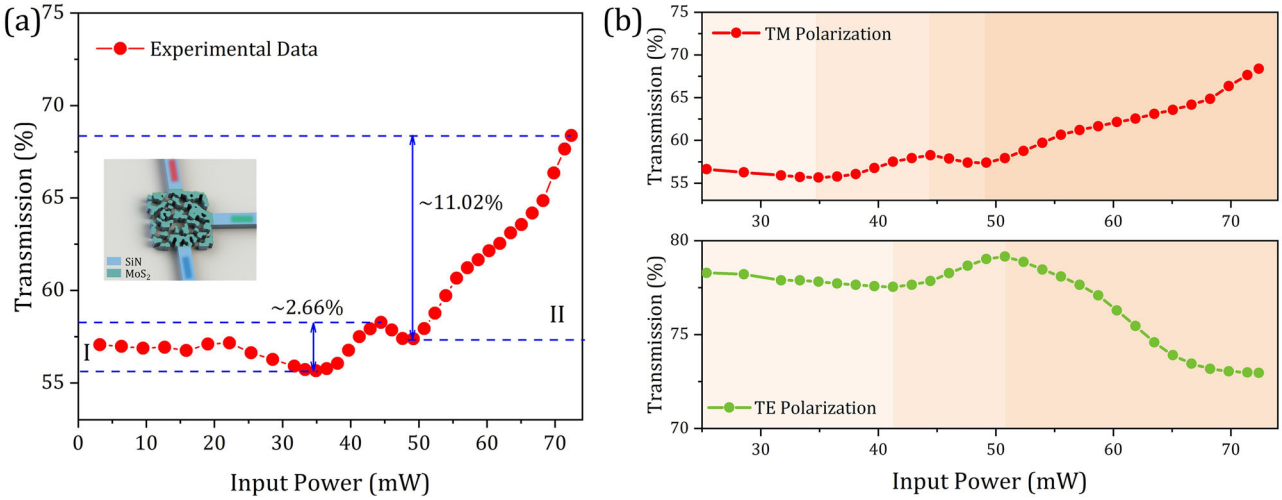

Figure 6. a) The transmission of TM polarized light to port 2 at different incident powers, corresponding the inverse-designed region fully cladded with few-layer MoS_2. b) Comparison of transmission curves of port 2 at TM and TE polarized incident lights, respectively. The gradient background colors represent different nonlinear optical response states.

Table 1. Comparison of the nonlinear optical response of the optical switch with and without the MoS_2 cladding.

Structure	State I			State II		
	Threshold [mW]	Modulation depth [%]	Saturation	Threshold [mW]	Modulation depth [%]	Saturation
Without MoS_2 cladding	34.91	13.56	Yes	53.96	9.09	Yes
With MoS_2 cladding	34.91	2.66	Yes	49.20	11.02	No

SiN material itself. At the second state II, the threshold of nonlinear optical response is lower than that of optical switch without MoS_2 cladding. The modulation depth is calculated to be 11.02%, which is comparable to the performance of optical switch without MoS_2 cladding and no apparent saturation is observed as the incident power increased to the maximum. Additionally, the integrated optical switch cladded with MoS_2 film also shows significant polarization-dependent transmission features. As shown in Figure 6b, when the polarization of incident light is set to be the TE mode, the transmission curve of port 2 in whole power range can be mainly divided into three parts. The overall trend is similar to that of optical switch without MoS_2 cladding. According to the simulated result of the optical field distribution in SiN waveguide (Figure S6, Supporting Information), the overlap between propagation light and MoS_2 is larger at TM polarized light than that of at TE polarized light, which indicates that MoS_2 film induces a stronger nonlinear enhancement at TM polarization and further achieves a large nonlinear modulation capability at high incident powers.

Table 1 shows the comparison of the nonlinear optical response of the integrated optical switch with and without the MoS_2 cladding. Interestingly, when the nonlinear optical response is at the first state I, the threshold is same between optical switch with and without MoS_2 cladding. The modulation depth of optical switch without MoS_2 cladding is near 5 times larger (13.56%) than that of the optical switch with MoS_2 cladding. The low modulation depth might be caused by the insertion loss during the transfer process and the linear absorption of few-layer MoS_2. In addition, both of two type devices show obvious nonlinear saturation at the first state. The results also indicate that the incident power at first state does not reach the nonlinear optical response threshold of MoS_2 film. In contrast, the integrated optical switch without MoS_2 cladding operates in saturation when the incident power is higher than 63.48 mW. However, the MoS_2 cladded integrated optical switch shows no apparent saturable trend even at the maximum incident power, indicating that the nonlinear optical response of integrated optical switch can be enhanced by few-layer MoS_2 effectively at high incident power. Furthermore, the carrier relaxation time of MoS_2 was reported at pico-second time scale,[36] indicating that MoS_2/SiN composite structure also has the potential for sub-nanosecond switching capability.

6. Conclusion

We demonstrate an integrated nonlinear optical switch designed by using inverse-design method combined with the Kerr-nonlinearity to maximum the value of objective function and experimentally characterized on the thick SiN platform. The integrated optical switch has an ultracompact footprint and shows significant intensity-dependent properties at different incident powers. The inverse-designed optical switch is also demonstrated to be polarization sensitive, which displays opposite transmission change trends at TE and TM polarized incident light, respectively. Furthermore, the demonstrated enhancement of nonlinear

optical performance by hybrid integrating vdWhs between few-layer MoS_2 and SiN devices could open routes to a range of novel applications with these 2DLMs and enable large-capacity photonic systems with high integration-density and ultrafast response time. The integrated ultrafast optical switch proposed in our experiment only relies on the Kerr-nonlinearity that is present in all materials, thus reducing fabrication complexity and eliminating the need for electrical connections, which opens many possibilities in on-chip lasers as artificial saturable absorbers, large-capacity optical communications, and large-scale integrated photonic circuits.[37–39]

Supporting Information

Supporting Information is available from the Wiley Online Library or from the author.

Acknowledgements

This work was supported by National Natural Science Foundation of China (61775146, 60907003, 61805278, and 62105371) and Shenzhen Science and Technology Project (JCYJ20190808174201658). This work was performed in part at the Photonics Center of Shenzhen University.

Conflict of Interest

The authors declare no conflict of interest.

Data Availability Statement

The data that support the findings of this study are available from the corresponding author upon reasonable request.

Keywords

2D layered materials, integrated photonics, inverse design, nonlinear optics, silicon nitride

Received: April 15, 2022
Revised: June 26, 2022
Published online:

[1] B. E. Little, S. T. Chu, *Opt. Photonics News* **2000**, *11*, 24.
[2] Q. Cheng, M. Bahadori, M. Glick, S. Rumley, K. Bergman, *Optica* **2018**, *5*, 1354.
[3] S. A. Miller, Y.-C. Chang, C. T. Phare, M. C. Shin, M. Zadka, S. P. Roberts, B. Stern, X. Ji, A. Mohanty, O. A. Jimenez Gordillo, U. D. Dave, M. Lipson, *Optica* **2020**, *7*, 3.
[4] A. H. Safavi-Naeini, D. Van Thourhout, R. Baets, R. Van Laer, *Optica* **2019**, *6*, 213.
[5] P. Cheben, R. Halir, J. H. Schmid, H. A. Atwater, D. R. Smith, *Nature* **2018**, *560*, 565.
[6] P. Dong, Y.-K. Chen, G.-H. Duan, D. T. Neilson, *Nanophotonics* **2014**, *3*, 215.
[7] R. Stabile, A. Albores-Mejia, A. Rohit, K. A. Williams, *Microsyst. Nanoeng.* **2016**, *2*, 15042.
[8] Z. Wang, Z. Wang, J. Xu, P. Yang, L. H. K. Duong, Z. Wang, H. Li, R. K. V. Maeda, *J. Lightwave Technol.* **2016**, *34*, 4364.
[9] D. Marpaung, J. Yao, J. Capmany, *Nat. Photonics* **2019**, *13*, 80.
[10] Z. Wang, J. Xu, P. Yang, Z. Wang, L. H. K. Duong, X. Chen, *J. Lightwave Technol.* **2017**, *35*, 4268.
[11] A. Kazmierczak, W. Bogaerts, E. Drouard, F. Dortu, P. Rojo-Romeo, F. Gaffiot, D. Van Thourhout, D. Giannone, *J. Lightwave Technol.* **2009**, *27*, 3317.
[12] M. Enachescu, Y. Ganjali, A. Goel, N. McKeown, T. Roughgarden, *ACM SIGCOMM Comput. Commun. Rev.* **2005**, *35*, 83.
[13] F. Riboli, N. Daldosso, G. Pucker, A. Lui, L. Pavesi, *IEEE J. Quantum Electron.* **2005**, *41*, 1197.
[14] D. M. Beggs, T. P. White, L. Cairns, L. O'Faolain, T. F. Krauss, *Phys. E* **2009**, *41*, 1111.
[15] X. Xue, Y. Xuan, C. Wang, P. H. Wang, Y. Liu, B. Niu, D. E. Leaird, M. Qi, A. M. Weiner, *Opt. Express* **2016**, *24*, 687.
[16] S. So, T. Badloe, J. Noh, J. Bravo-Abad, J. Rho, *Nanophotonics* **2020**, *9*, 1041.
[17] C. Sideris, E. Garza, O. P. Bruno, *ACS Photonics* **2019**, *6*, 3233.
[18] D. Liu, Y. Tan, E. Khoram, Z. Yu, *ACS Photonics* **2018**, *5*, 1365.
[19] A. Y. Piggott, J. Lu, K. G. Lagoudakis, J. Petykiewicz, T. M. Babinec, J. Vučković, *Nat. Photonics* **2015**, *9*, 374.
[20] S. Molesky, Z. Lin, A. Y. Piggott, W. Jin, J. Vucković, A. W. Rodriguez, *Nat. Photonics* **2018**, *12*, 659.
[21] T. W. Hughes, M. Minkov, I. A. D. Williamson, S. Fan, *ACS Photonics* **2018**, *5*, 4781.
[22] A. Autere, H. Jussila, Y. Dai, Y. Wang, H. Lipsanen, Z. Sun, *Adv. Mater.* **2018**, *30*, 1705963.
[23] Z. Sun, A. Martinez, F. Wang, *Nat. Photonics* **2016**, *10*, 227.
[24] J. W. You, S. R. Bongu, Q. Bao, N. C. Panoiu, *Nanophotonics* **2018**, *8*, 63.
[25] S. Yu, X. Wu, Y. Wang, X. Guo, L. Tong, *Adv. Mater.* **2017**, *29*, 1606128.
[26] E. P. Nguyen, B. J. Carey, J. Z. Ou, J. van Embden, E. D. Gaspera, A. F. Chrimes, M. J. Spencer, S. Zhuiykov, K. Kalantar-Zadeh, T. Daeneke, *Adv. Mater.* **2015**, *27*, 6225.
[27] Y. Liu, Y. Huang, X. Duan, *Nature* **2019**, *567*, 323.
[28] D. Jariwala, T. J. Marks, M. C. Hersam, *Nat. Mater.* **2017**, *16*, 170.
[29] L. Liu, K. Xu, X. Wan, J. Xu, C. Y. Wong, H. K. Tsang, *Photonics Res.* **2015**, *3*, 206.
[30] D. Perez-Lopez, A. Gutierrez, J. Capmany, *Opt. Express* **2021**, *29*, 9043.
[31] B. Shen, L. Chang, J. Liu, H. Wang, Q. F. Yang, C. Xiang, R. N. Wang, J. He, T. Liu, W. Xie, J. Guo, D. Kinghorn, L. Wu, Q. X. Ji, T. J. Kippenberg, K. Vahala, J. E. Bowers, *Nature* **2020**, *582*, 365.
[32] B. Stern, X. Ji, Y. Okawachi, A. L. Gaeta, M. Lipson, *Nature* **2018**, *562*, 401.
[33] J. Liu, A. S. Raja, M. H. P. Pfeiffer, C. Herkommer, H. Guo, M. Zervas, M. Geiselmann, T. J. Kippenberg, *Opt. Lett.* **2018**, *43*, 3200.
[34] K. Shtyrkova, P. T. Callahan, M. R. Watts, E. P. Ippen, F. X. Kärtner, in Conf. Lasers and Electro-Optics, OSA Technical Digest, Optica Publishing Group, Washington **2017**, paper AF1B.6.
[35] H. Ballani, P. Costa, I. Haller, K. Jozwik, K. Shi, B. Thomsen, H. Williams, in Optical Fiber Communication Conf., *OSA Technical Digest*, Optica Publishing Group, Washington **2018**, paper W1C.3.
[36] H. Chen, X. Wen, J. Zhang, T. Wu, Y. Gong, X. Zhang, J. Yuan, C. Yi, J. Lou, P. M. Ajayan, W. Zhuang, G. Zhang, J. Zheng, *Nat. Commun.* **2016**, *7*, 12512.
[37] Z. Sun, T. Hasan, F. Torrisi, D. Popa, G. Privitera, F. Wang, F. Bonaccorso, D. Basko, A. C. Ferrari, *ACS Nano* **2010**, *4*, 803.
[38] M. Zhang, R. Howe, R. Woodward, E. Kelleher, F. Torrisi, G. Hu, S. Popov, J. Taylor, T. Hasan, *Nano Res.* **2015**, *8*, 1522.
[39] G. Wang, A. A. Baker-Murray, W. J. Blau, *Laser Photonics Rev.* **2019**, *13*, 1800282.